https://doi.org/10.5194/nhess-2023-119
Preprint. Discussion started: 8 August 2023


Natural Hazards and Earth System Sciences
Discussions

# Comparison of different rheological approaches and flow direction algorithms in a physically based debris flow model for data scarce regions

Leonardo Rodolfo Paul[1], Gean Paulo Michel[1], Heron Schwarz[1], Bruno Henrique Abatti[1], Clarissa Guerra Salvador[1]

[1] Instituto de Pesquisas Hidráulicas, Universidade Federal do Rio Grande do Sul, Porto Alegre (RS), Brazil

*Correspondence to:* Leonardo Rodolfo Paul (leonardorpaul@gmail.com), Gean Paulo Michel (gean.michel@ufrgs.br)

**Abstract.** A debris flow simulation model was proposed for data-scarce regions. The model couples a one-dimensional explicit solution for a monophasic sediment-water mixture with flow direction algorithms for debris flow routing. We investigate the effects of different multiple flow direction algorithms (D8, D∞, and Freeman's Multiple Flow Direction (MFD)) and multiple rheology approaches (Newtonian, Bingham, Herschel-Bulkley, and dilatant) for the one-dimensional flow on the debris flow simulations. The model was tested by simulating debris flows triggered by an extreme rainfall in the Mascarada river basin in southern Brazil. We conducted two separate sets of simulations: one focused on the effects of flow directions, considering multiple DEM resolutions, and another to compare rheology approaches. A third simulation was conducted for multiple debris flows concurrently, utilizing optimal parameters derived from the results of the two simulation sets. D8 proved to be unsuitable for debris flow routing, whereas MFD performed better for high-resolution DEM (1 m pixel size) and D∞ for coarser resolutions (2.5, 5, and 10 m). In terms of affected area, the difference between the rheology approaches was less impactful than the difference between flow direction algorithms. The lack of velocity estimates and deposition depths for the simulated debris flow hindered a detailed comparison of which rheology had a more accurate result. Nevertheless, we found MFD and dilatant fluid to perform slightly better and utilize the optimal parameters to simulate three other debris flows, reaching true positive ratios of 58% up to 83%.

## 1 Introduction

Landslide driven debris flows are natural processes of landscape evolution that could lead to severe impacts when occurring near populated areas. Identifying areas prone to the effects of debris flow is essential to reduce loss of lives and damage to public and private properties. In some developing countries, advances and/or efforts towards the understanding of debris flow processes tend to be lacking. Consequently, a scenario of data scarcity is created with a poor debris flow inventory and limited capacity to identify areas of debris flow hazard (Frey et al., 2016). For instance, in Brazil there are not many detailed records of debris flow (Cabral et al., 2023) despite of the occurrence of high magnitude debris flow disasters (Kobiyama et al., 2019). Debris flows that were recorded frequently lack information such as soil characteristics, volume estimates of the deposits, and timing of occurrence. In this context, there are situations where neither robust physically based model (e.g., Pitman et al., 2003; Liu and Huang, 2006; Nakatani et al., 2008; Pirulli and Sorbino, 2008; Liu and He, 2020) or data driven methodologies (e.g., Melo and Zêzere, 2017; Steger et al., 2022; Zhang et al., 2019) could be effectively applied to identify areas prone to the effects of debris flows. The implementation of some empirical and/or statistical models (e.g., Tang et

https://doi.org/10.5194/nhess-2023-119
Preprint. Discussion started: 8 August 2023


Natural Hazards and Earth System Sciences
Discussions

al., 2012; Horton et al., 2013; Berti and Simoni, 2014; Gorr et al., 2022) could be a solution for data scarce regions, since they can show good results and are reasonably simple to use. Despite this simplicity, empirical relationships may not be applicable to regions where geomorphological settings, biomes, and triggering mechanisms differ from those found in the data used to develop them (Hürlimann et al., 2008; Cabral et al., 2021). Thus, a model that seeks to represent the debris process with physical equations and little parametrization is of interest for data scarce regions.

Some recent studies, such as Abraham et al. (2022), approach debris flow simulation focusing on maintaining as few input parameters as possible, with some simplifications of the equations. Chiang et al. (2012) proposed a debris flow runout model built on physically based equations with explicit solutions. The model assumptions reduce the calibration to a single parameter - the kinematic viscosity. The approach showed promising results, providing information of affected area, deposition depth and reached velocities even with few inputs. The methodology utilizes one-dimensional Newtonian solutions coupled with flow direction algorithms. However, debris flows are known for their non-Newtonian behavior, which vary depending on factors such as sediment concentration, granulometry and soil mechanical parameters (Phillips and Davies, 1991; Kaitna et al., 2007; Pellegrino and Schippa , 2018). Different approaches to rheology had been employed to simulate debris flows, e.g., Bingham (Chen and Lee, 2002), Voellmy (Naef et al., 2006; Rickenmann et al., 2006), Herschel-Bulkley (Huang and Garcia, 1998; Han et al., 2019; Schippa, 2020), and dilatant (Takahashi, 2014). Furthermore, as velocities are calculated in one dimension, a solution to distribute the flow over a two-dimensional grid is based on flow direction algorithms (FDA). FDA are normally employed to calculate flow accumulation areas through the delineation of a topographic-based flow path. Chiang et al. (2012) used $D_\infty$ (Tarboton, 1997), widely used for hydrological analysis with digital elevation models (DEM). However, there are other widely known approaches to flow directions, e.g., deterministic eight (D8) by O'Callaghan and Mark (1988) and multiple flow direction (MFD) by Freeman (1991), that have yet to be tested in this model framework.

Thus, based on the framework presented by Chiang et al. (2012), we developed a model containing multiple methodologies for determining flow direction (D8, $D_\infty$, and Freeman's MFD) and one-dimensional rheology approaches (Newtonian, Bingham, generalized Herschel-Bulkley, and dilatant) to compare their effects on debris flow simulations. We conducted sets of simulations for a debris flow that occurred in January 2017 in the Mascarada River Basin, Southern Brazil, to evaluate the difference between these methodologies. Also, we found the best combination of FDA and rheology to reconstruct the 2017 Mascarada event and simulated other debris flows in the region to validate the model.

## 2 Methods

The grid-based model utilized in this study is based on Chiang et al. (2012) debris flow routing method. The model utilizes a pre-processed DEM to determine the flow path and calculates the volume flowing outwards of a cell based on flow height. The simulation ends when the difference of height between time steps in all cells are inferior to a predetermined value – for this study a value of 1 cm was used for time steps of 1 s, indicating very low flow velocities. The model was developed in Python 3.7. To test the effects of flow direction algorithms on the simulation routes and effects of rheological approaches on the velocity's calculations, two different sets of simulations were performed. The first set utilizes the Newtonian approach, following Chiang et al. (2012)

https://doi.org/10.5194/nhess-2023-119
Preprint. Discussion started: 8 August 2023




framework and test the effects of flow direction algorithms. In the second set, the optimal flow direction algorithm is paired with different rheological approaches that were not priorly tested in this model framework. A flowchart summarizing the methodology is shown in Figure 1.

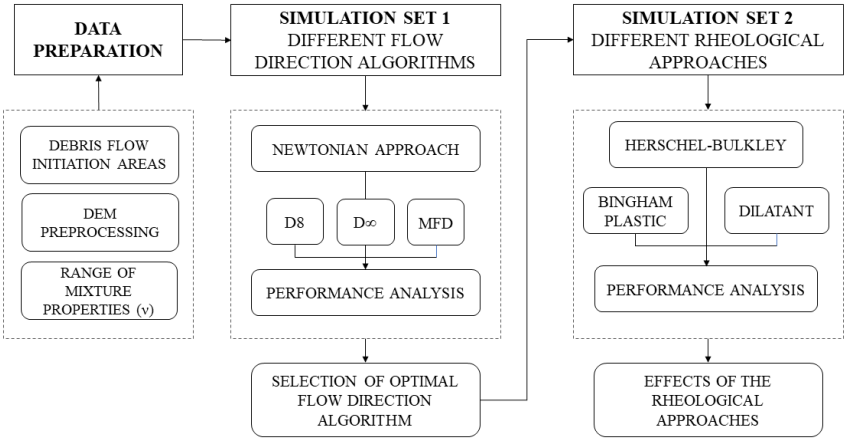


**Figure 1:** Study's methodology flowchart

### 2.1 Calculation of the unitary flow

The calculation of the unitary flow is based on the constitutive equations for Newtonian, Bingham, dilatant, and generalized Herschel-Bulkley fluids. The equations of Bingham, dilatant, and generalized Herschel-Bulkley can be easily solved in the same manner as Hunt's (1994) approach to laminar Newtonian debris flow. The Newtonian approach was utilized to observe the effects of different flow direction algorithms on the representation of debris flow in the first set of simulations. The other rheological approaches are employed on the second set of simulations to compare their effects on volume distribution.

The model has the following basic assumptions and some inherent limitations:

i) Fully developed steady uniform flow.
ii) Laminar flow.
iii) Monophasic mixture.
iv) The cells have rectangular cross sections.
v) The volume is uniformly distributed in a cell, and it is a function of the flow height.
vi) The outflow and inflow of a cell occur simultaneously.
vii) The outflow of a cell cannot surpass the existing volume in *t*-1.
viii) Neglects formation of permanent or temporary obstacles (e.g., damming/channel constriction).
ix) Does not consider bed erosion, particle entrainment and particle deposition.
x) Does not consider water gain or loss during the simulation. Thus, channel water discharge won't contribute to the debris flow volume.

https://doi.org/10.5194/nhess-2023-119
Preprint. Discussion started: 8 August 2023


Natural Hazards and Earth System Sciences
Discussions

xi) Does not consider runup, breaching and other debris flow interactions with structures.

xii) Outflow is set to zero in cells with flow depths inferior to 0,1 mm. Flows related to this value are negligible if the time step of the calculation is high enough. Furthermore, the 0,1 mm is utilized as threshold in the code to identify unactive cells during algorithm calculations.

xiii) Time step for calculations is a fixed value.

Particle entrainment, bed erosion and deposition are important processes to be considered in debris flow modeling. However, to keep the model with the lowest parametrization possible to keep it feasible in data scarce regions, they are not included in the model. The implications of these simplifications are discussed later.

#### 2.1.1 Newtonian

The Newtonian approach to debris flow is based on Hunt (1994). The solution is obtained from Navier-Stokes equations for two dimensions, assuming a parabolic velocity profile:

$$u = \frac{g}{2\nu_N}[h^2 - (h-y)^2]\sin\theta \quad (1)$$

$u$ is the is the velocity parallel to the surface [m/s] in the $y$ position of the vertical component; $\nu_N=\mu/\rho$ is the Newtonian kinematic viscosity [m²/s], being $\rho$ the fluid density [kg/m³]; $g$ is the gravity acceleration [m/s²]; $h$ is the flow height [m]; $\theta$ is the slope angle [°]. Considering a flow with a maximum depth of $h$, the unitary flow ($q$ [m²/s]) can be determined through integration of the variation of velocity along the vertical component:

$$q = \int_0^h u\,\partial y = \frac{gh^3}{3\nu_N}\sin\theta \quad (2)$$

The mean velocity ($U$) is given by:

$$U = \frac{q}{h} = \frac{gh^2}{3\nu_N}\sin\theta \quad (3)$$

#### 2.1.2 Bingham plastic

Bingham plastics only start to strain at a given shear stress value, the yield stress ($\tau_y$). Therefore, the strain rate for Bingham plastic is expressed by:

$$\mu_b\left(\frac{\partial u}{\partial y}\right) = \begin{cases} 0, & \tau < \tau_y \\ \tau - \tau_y, & \tau \geq \tau_y \end{cases} \quad (4)$$

Based on Jan e Shen (1997), the velocity profile, unitary flow, and mean velocity with constant values of $\tau_y$ and $\mu_b$ in a steady and uniform flow are expressed respectively by:

$$u = \frac{g\cdot(h-z')^2\cdot\sin\theta}{\nu_B}\left[\frac{y}{h-z'} - \frac{1}{2}\left(\frac{y}{h-z'}\right)^2\right] \quad (5)$$

$$q = \int_0^{z'} u\,\partial y = \frac{g\cdot(h-z')^3\sin\theta}{\nu_B}\left(\frac{1}{2} - \frac{(h-z')}{6h}\right) \quad (6)$$

https://doi.org/10.5194/nhess-2023-119
Preprint. Discussion started: 8 August 2023




$$U_B = \frac{g \cdot (h-z')^2 \sin\theta}{\nu_B}\left(\frac{1}{2} - \frac{(h-z')}{6h}\right) \quad (7)$$

$z'$ adapts fluid's yield stress in function of a plug height [m], therefore flow depths equal or below $z'$ result in $U = 0$; $\nu_B$ and $U_B$ are respectively kinematic viscosity and mean velocity for Bingham fluid.

### 2.1.3 Herschel-Bulkley

Herschel-Bulkley fluid has a non-linear stress-strain relationship and has a yield stress to start to flow:

$$K_{HB}\left(\frac{\partial u}{\partial z}\right)^m = \begin{cases} 0, & \tau < \tau_y \\ \tau - \tau_y, & \tau \geq \tau_y \end{cases} \quad (8)$$

where $K_{HB}$ is Heschel-Bulkley's consistency index, $m$ is the flow index. Based on Jan e Shen (1997), velocity profile and mean velocities ($U_{HB}$) are expressed by:

$$u = \left(\frac{m}{m+1}\right)\left(\frac{g \cdot (h-z')^{m+1} \cdot \sin\theta}{\nu_{HB}}\right)^{\frac{1}{m}}\left[1 - \left(1 - \frac{y}{h-z'}\right)^{\frac{m+1}{m}}\right] \quad (9)$$

$$U_{HB} = \left(\frac{m}{m+1}\right)\left(\frac{g \cdot (h-z')^{m+1} \cdot \sin\theta}{\nu_{HB}}\right)^{\frac{1}{m}}\left(1 - \frac{m}{2m+1}\frac{h-z'}{h}\right) \quad (10)$$

where $\nu_{HB} = K_{HB}/\rho$.

### 2.1.4 Dilatant

Dilatant fluids resist deformation as shear stress increases. Based on the rheological constitutive equation, for a steady and uniform flow, velocity profile and mean velocity ($U_D$) are expressed by the following equations:

$$u = \left(\frac{n}{n+1}\right)\left(\frac{g \cdot h^{n+1} \cdot \sin\theta}{\nu_D}\right)^{\frac{1}{n}}\left[1 - \left(1 - \frac{y}{h}\right)^{\frac{n+1}{n}}\right] \quad (11)$$

$$U_D = \left(\frac{n}{n+1}\right)\left(\frac{g \cdot h^{n+1} \cdot \sin\theta}{\nu_D}\right)^{\frac{1}{n}}\left(1 - \frac{n}{2n+1}\right) \quad (12)$$

Where $\nu_D = K_D/\rho$ and $K_D$ is the consistency factor for dilatant fluid. Equation (11) and Eq. (12) were deduced following general Herschel-Bulkley formulations from Jan and Shen (1997). More information can be found in Appendix A.

## 2.2 Determination of the flow direction

https://doi.org/10.5194/nhess-2023-119
Preprint. Discussion started: 8 August 2023


Natural Hazards and Earth System Sciences
Discussions

The unitary flow is transported to the next cell based on the routes determined by the flow direction algorithm. This study utilized three different flow direction methods: (i) Deterministic eight – D8 (O'Callaghan and Mark, 1984), distributes the flow from a pixel to a single direction over 8 possibilities (8 surrounding cells); (ii) $D_\infty$ (Tarboton, 1997) indicates a single direction over infinite possibilities based on the steepest slope and can partition the flow up to two cells; (iii) Freeman's (1991) Multiple Flow Direction (MFD), that distributes the flow to all cells that have lower elevation than the analyzed pixel – the volumes are partitioned proportionally to the slope between the central pixel and the neighbor cell. To evaluate flow depth changes for each time step, the following mass balance equation is utilized:

$$\frac{\partial h}{\partial t} + \nabla q = 0 \tag{13}$$

Equation (13) expresses a balance of inflows and outflows of a cell linked to the eight surrounding cells. Discretizing the equation by finite difference, the flow depth of a cell given a time *t* is expressed by:

$$h(t) = h(t-1) + \frac{\Delta t}{b}\left(\sum_{i=1}^{8} q_{in} - \sum_{i=1}^{8} q_{out}\right) \tag{14}$$

*b* is the cell size [m]; $q_{in}$ is the inflow [m²/s]; $q_{out}$ [m²/s] the outflow.

**2.3 Performance analysis**

The following metrics were utilized to assess the model performance, allowing objective comparison between simulations with different flow direction methods, DEM resolutions and rheological approaches:

i) Heidke's score (*Hs*) (Heidke, 1926) – based on de Frattini et al. (2010) – measure the correct classification fraction and eliminates correct classifications due to randomness:

$$Hs = \frac{TP + TN - E}{T - E} \tag{15}$$

$$E = \frac{1}{T}\left[(TP + FN)(TP + FP) + (TN + FN)(TN + FP)\right] \tag{16}$$

*TP*, *TN*, *FP*, and *FN* are respectively true positive, true negative, false positive and false negative, *E* is the estimate of correct classifications due to randomness; *T* is the total of analyzed pixels. A perfect simulation has a $H_S$ of 1. We considered only the observed affected area as the observed positive individuals and a binary based classification (either affected or not affected by the debris flow simulation). As the domain is mostly composed of negative individuals, a great fraction of the area won't be reached by the simulated debris flow. This could lead to a false notion of good performance and hinder performance comparison for simulation over different areas. The total negatives were set to be at a maximum of five times the total positives, as done by Mergili et al. (2015). In addition, the debris flow initiation areas were not considered as true positives for model evaluation and their pixel count were removed from the analyses.

ii) True positive ratio (*TPR*) – ratio of positive classifications inside the debris flow scar:

https://doi.org/10.5194/nhess-2023-119
Preprint. Discussion started: 8 August 2023




$$TPR = \frac{TP}{TP + FN} \quad (17)$$

iii) False positive ratio (*FPR*) – number of pixels mistakenly classified as positives:

$$FPR = \frac{FP}{FP + TN} \quad (18)$$

iv) False negative ratio (*FNR*) – ratio of false negatives inside debris flow scar:

$$FNR = \frac{FN}{TP + FN} = 1 - TPR \quad (19)$$

v) False discovery ratio (*FDR*) – indicates overestimation of results by the fraction of positive classifications that extrapolates observed positives:

$$FDR = \frac{FP}{FP + VP} \quad (20)$$

## 3 Study area

### 3.1 The debris flow event of Mascarada river basin

The Mascarada river basin is in the Southern region of Brazil, in Rio Grande do Sul state (Figure 2) with an area of 318.2 km$^2$. The basin has an elevation amplitude of 938 m and slopes ranging from 0° to 85°, with a 10° to 35° predominance.

On January 5th, 2017, an extreme rainfall event occurred, triggering over 400 landslides and debris flows along the watershed (Cardozo, 2021; Schwarz et al., 2023). Despite the lack of official or automated pluviometers in the affected region, unofficial measurements done by farmers on simple bucket rain gauges accounted for up to 272 mm in a few hours (SEMA, 2017). Although most of the precipitation was contained in the basin's headwaters, a few hours after the landslides triggered, a sudden flood heavily concentrated with sediments, reached the nearest municipality, located directly downstream of the triggered hillslopes. During field surveys, carried out shortly after the event, evidence of debris flow-induced valley blockage was found along the Mascarada river. Also, a high amount of wood and rock debris were observed (Figure 3). Most of landslides were triggered in the basin's middle to upper reaches, in a region also known as the escarpments of Serra Geral formation. The escarpments are a transition zone with steep slopes between the Serra Geral plateau and the coastal plains, characteristically defined by the steep slopes.

As result of the high declivity hillslopes and enclosed valleys, the majority of the debris flows reached the channel, making the delineation of the deposition zones more difficult. Furthermore, as we have few observations during the event, it was not possible to verify to what extent the debris flows continued with similar behavior after reaching the channel. To reduce uncertainties inherent to the lack of data, this research was focused on the simulation of debris flows that did not reach the channel and, in this way, that could be fully mapped from its initiation to the deposition zone.

https://doi.org/10.5194/nhess-2023-119
Preprint. Discussion started: 8 August 2023


Natural Hazards and Earth System Sciences
Discussions

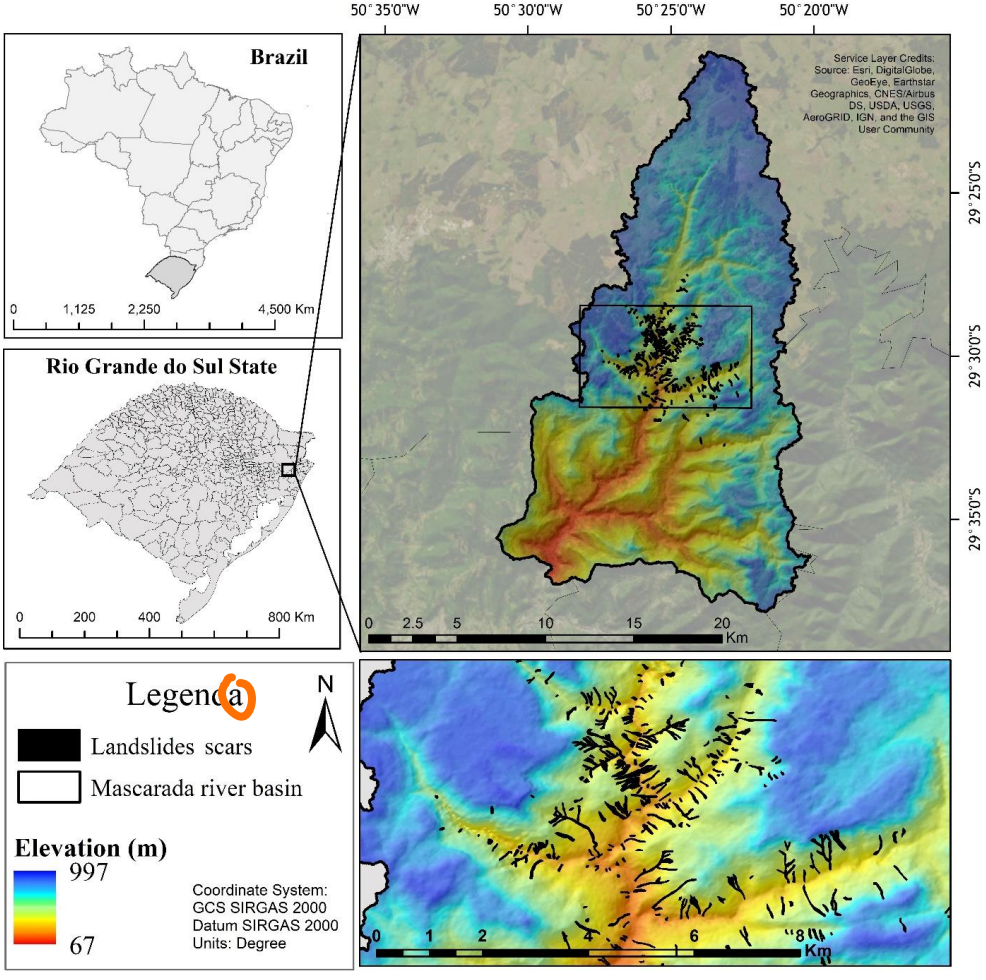


195 **Figure 2: Location and altimetry of Mascarada river basin with landslide scars**

**Figure 3: Left: debris flow deposits in the Mascarada river; right: evidence of woody debris (Kobiyama et al., 2017)**

https://doi.org/10.5194/nhess-2023-119
Preprint. Discussion started: 8 August 2023




### 3.2 Model inputs and data

The utilized digital elevation model (DEM) has 1 m horizontal resolution. It has a vertical and horizontal accuracy of 2 m root-mean-square error (RMSE)/3 m LE90 (absolute) and 1 m RMSE/1.5 m LE90 (relative). This DTM is the AW3D Enhanced acquired from NTT DATA Corporation. Since the model cannot estimate flow velocities without slope values and may accumulate unrealistic volumes in pits due to flow convergences, DEM pits were filled. To test the resolution effects on the model, the DEM was downscaled to 2.5 m, 5 m, and 10 m resolution using bilinear interpolation.

The debris flow scars that did not reach the channel were identified using Cardozo et al. (2021) landslide inventory. Four debris flows were simulated in total, three of which did not connect to the Mascarada River. According to the information provided in a technical report by the Secretaria do Meio Ambiente e Infraestrutura, SEMA (2017), the soil depth for the initiation zones is assumed to be 1 m.

Based on the amplitude of measured rheological parameters of debris flow from Phillips and Davies (1991) study, which collect data from different studies and summarizes the ranges of measured rheological parameters, the kinematic viscosity values ranged from $1\times10^{-5}$ to 1 $m^2/s$ considering a soil with density of 2.65 $kg/m^3$. The parameters $n$ and $m$ are set empirically. The $z'$ was set empirically after a few tests as a maximum of 10% of the initial flow height for the debris flow utilized in this study, thus $z'_{MAX} = 0.1$ m), since high values of $z`$ (above 20%) were ending the simulation after few iterations, barely moving the debris flow volumes. The flow partition exponent, which controls MFD spreading, was set empirically to 1.5 based on a set of tests – higher values lead to less spreading and ranges from 1 to +∞, in which +∞ makes the algorithm behave similarly to D8. The model also requires a grid of debris flow initiation areas with initial flow depths in meters, and a DEM. Table 1 summarizes the input parameters.

https://doi.org/10.5194/nhess-2023-119
Preprint. Discussion started: 8 August 2023


Natural Hazards and Earth System Sciences
Discussions

**Table 1: Physical and operational parameter inputs**

| | PARAMETER | VALUE | UNITS | METHOD |
|---|---|---|---|---|
| Physical | n | 1.2 - 2.0 | - | Dilatant |
| | m | 0.6 - 1.4 | - | HB |
| | z' | 2.5 - 10.0 | cm | HB, Bingham |
| | Consistency factor/Mixture density | $1.0\times10^{-4}$ - 1.0 | $m^2/s$ | - |
| | Initial flow depth | 1.0 | m | - |
| Operational | Time step | 1.0 | s | - |
| | Flow partition exponent (η) | 1.5 | - | MFD |
| | Stop criteria (max Δh) | 0.01 | m | - |

## 4 Results

### 4.1 Simulations with different flow directions

The first set of simulations utilized a Newtonian approach to debris flow, focusing on the differences caused by the flow direction algorithms. Figure 4 shows a plot of simulation performance. Some simulations did not meet the stopping criteria after thousands of iterations, and others had a count of false positives higher than observed negatives (adapted to be 5 times the observed positives). These cases' performance could not be analyzed and are not included in the plot.

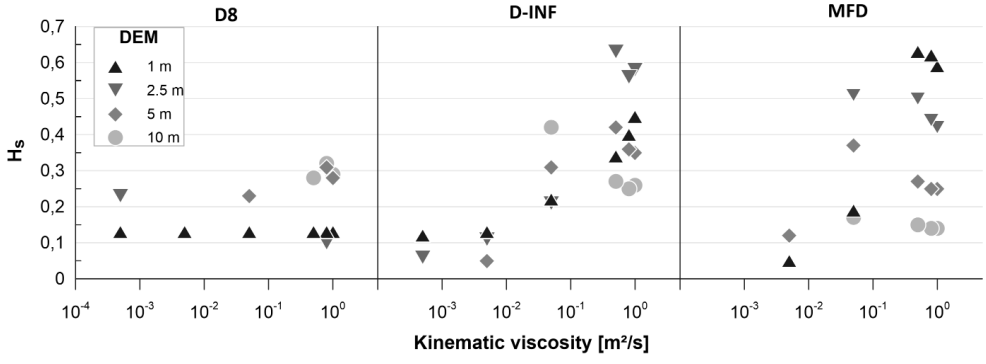


**Figure 4: $H_S$ for different flow direction algorithms**

D∞ and MFD performed better than D8, as indicated by the $H_S$. In terms of DEM resolutions, $D_\infty$ performed better with a 2.5 m DEM ($H_S$ up to 0.63), whereas MFD performed better with the original 1 m DEM ($H_S$ up to 0.63).

Figure 5 shows the simulations that performed better with a 1 m DEM for each flow direction method: D8 resulted in the same $H_S$ regardless of the kinematic viscosity since it reached the DEM edge; $D_\infty$ performance proportionally increased with kinematic viscosity, with the highest $H_S$ at 1 $m^2/s$; MFD performed better with kinematic viscosity of 0.5 $m^2/s$. Final depths for D8 (982 m) were unrealistically higher in the simulations displayed

https://doi.org/10.5194/nhess-2023-119
Preprint. Discussion started: 8 August 2023


Natural Hazards and Earth System Sciences
Discussions

in Figure 5, because it converged almost all initiation volume in a single cell at the DEM edge. The final depths of
245 $D_\infty$ and MFD, on the other hand, were less than 0.52 m and 1.90 m, respectively.

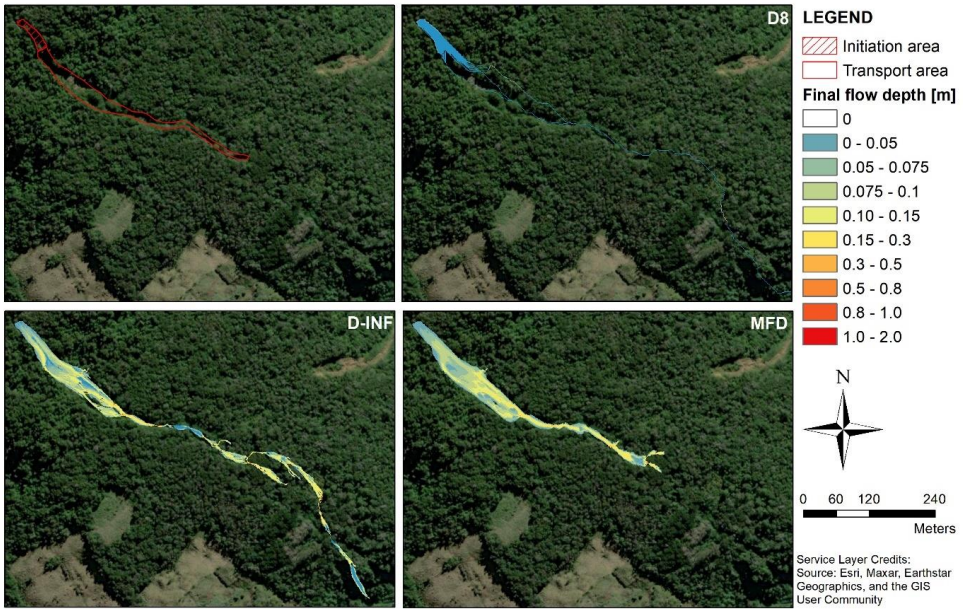


**Figure 5: Simulation with highest $H_S$ for D8, $D_\infty$ and MFD flow direction algorithm utilizing a 1 m x 1 m resolution DEM**

### 4.2 Simulations with different rheological approaches

250 Figures 6 and 7 show plots with simulations performance for different rheological approaches. MFD was used as the flow direction algorithm because it performed better when applied to the original 1m x 1 m DEM. The upper plot shows $H_S$ values for dilatant and Bingham simulations, while the lower plot displays $H_S$ for Herschel-Bulkley approach.

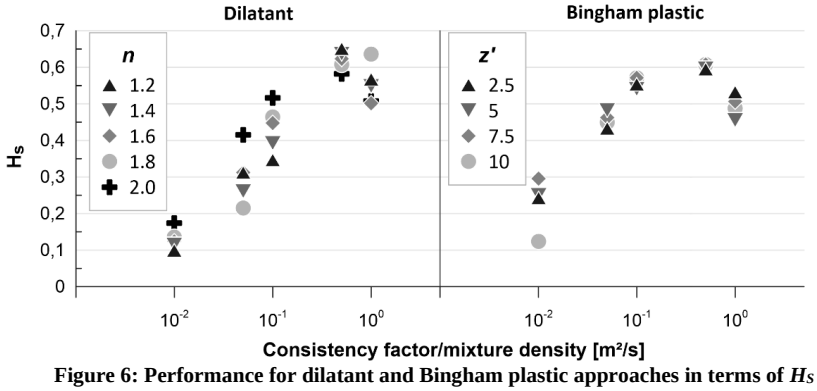


255 **Figure 6: Performance for dilatant and Bingham plastic approaches in terms of $H_S$**

https://doi.org/10.5194/nhess-2023-119
Preprint. Discussion started: 8 August 2023


Natural Hazards and Earth System Sciences
Discussions

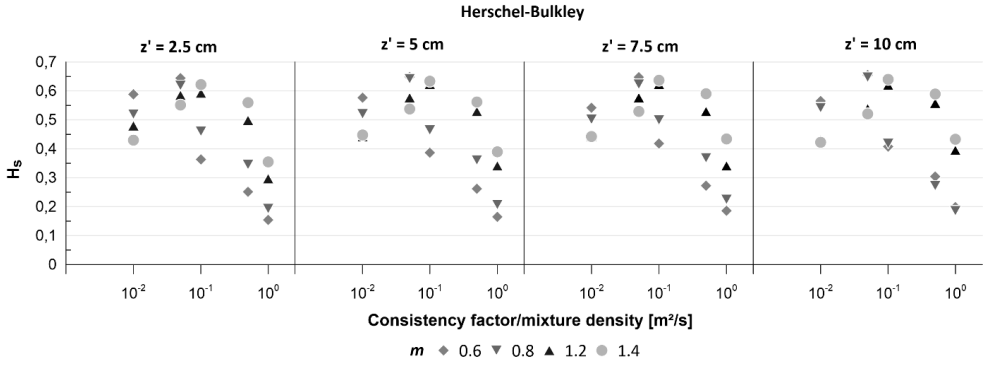


**Figure 7: Performance for dilatant and Bingham plastic approaches in terms of $H_S$**

Dilatant approach simulations resulted in $H_S$ values up to 0.65. The simulation performances were higher for $n$ of 1.2. For Bingham plastic, $H_S$ values are clustered together for the same $z'$, indicating little influence of this parameter over the simulated affected area. For Herschel-Bulkley approach, $H_S$ values tended to decrease with $m$ lower than 1 as the $v_{HB}$ increased. Conversely, $m > 1$ simulations had an increase for $v_{HB}$ up to 0.1 m$^2$/s, followed by a decrease as $v_{HB}$ increased. Furthermore, $H_S$ values had varied more for simulation sets with $m < 1$ than for those with $m > 1$.

### 4.3 Validation scenarios

Other debris flow simulations were carried out near the one used in previous tests. The dilatant with $n$ of 1.2 and $v_D = 0.5$ m$^2$/s had the highest $H_S$, thus, the best representation of the debris flow, so it was used as the basis for the input parameters. Table 2 shows the performance indices for each debris flow. F1 is the reference debris flow (utilized as a calibration subject); F2 and F3 were simulated concomitantly; F4 is a debris flow connected to the channel and, thus, does not have a discernible deposition zone.

The *TPR* and *FPR* from the F2 and F3 simulations were 84.06% and 17.25%, respectively. F4 performed poorly when compared to other debris flows, with a *TPR* of 58.2 percent and an *FDR* of 70.75 %. Furthermore, F4 caused a large accumulation of volume in a constriction near the middle of the observed scar as well as in the channel, with maximum final depths reaching 3.24 m. Figure 8 displays the debris flow depth at the end of the simulations.

**Table 2: Performance indexes for the simulated debris flow**

| Debris flow | *TPR* | *FPR* | *FDR* | *FNR* | *Hs* | Time (s) | Max. final depth (m) |
|---|---|---|---|---|---|---|---|
| F1 | 83.15 | 9.74 | 36.94 | 16.85 | 0.65 | 437 | 0.38 |
| F2 & F3 | 84.06 | 17.25 | 50.64 | 15.94 | 0.52 | 396 | 0.31 |
| F4 | 58.20 | 28.15 | 70.75 | 41.80 | 0.22 | 744 | 3.24 |

https://doi.org/10.5194/nhess-2023-119
Preprint. Discussion started: 8 August 2023


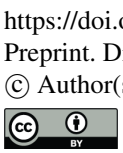

Natural Hazards and Earth System Sciences
Discussions
Open Access
EGU

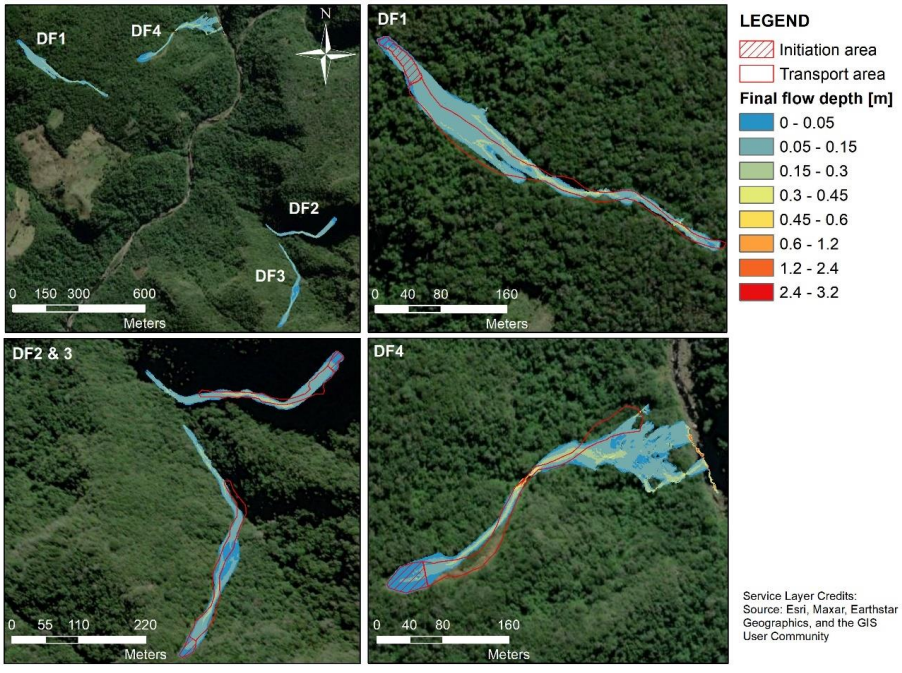


**Figure 8: Validation debris flow set simulated with the coupling of MFD and dilatant rheological approach**

## 5 Discussion

### 5.1 Simulations with different flow directions

The D8 performed poorly in all situations, not being able to portray the debris flow properly. Higher $H_S$ were obtained with the 2.5 m and 5 m DEM. The coarser resolution compensated for one of the D8 shortcomings: the flow's unrealistic convergence in a single path. The increased pixel area resulted in a higher true positive rate. Thus, lower resolutions outperformed the original 1 m DEM. The 10 m resolution reduced $H_S$ values, most likely due to changes in terrain caused by resampling. The dissimilarity between the observed scar and D8 simulations can be visually identified in the Figure 5.

$D_\infty$ simulations resulted in a more coherent shape than D8 simulations when compared to the observed transport area. Despite being also a single flow direction algorithm, $D_\infty$ can represent divergence of flows. Cavalli et al. (2013) opted for a $D_\infty$ instead of D8 and MFD methods to avoid grid bias and overspreading respectively. However, for debris flow simulation, $D_\infty$ resulted in two separate flow paths that only converged further down the slope, whereas the observed transport area does not indicate this behavior. Horton et al. (2013) states the $D_\infty$ limited spreading to two cells can be insufficient in some cases, especially in alluvial fans. Regarding DEM resolution, the $D_\infty$ performed better for cells with 2.5 m, reaching $H_S$ of 0.63 for the simulation with a kinematic viscosity of 0.5 $m^2/s$. At coarser resolutions, performance declines, particularly for higher viscosities – in most cases, the

https://doi.org/10.5194/nhess-2023-119
Preprint. Discussion started: 8 August 2023




simulation ended before reaching the landslide scar perimeter, indicating small volume exchanges between cells and, thus, lower velocities.

The MFD performed best for the original 1 m DEM. MFD's capability to distribute flow in any direction resulted in a transport zone with fewer voids along the transport area, in contrast to what was seen in D8 and $D_\infty$ simulations. Also, MFD resulted in a smoother distribution of flow heights, identified by a lower contrast between higher efficiency topographic flow paths and their neighboring cells, when compared to $D_\infty$. For coarser DEM resolutions, MFD performance declined significantly. Considering a kinematic viscosity of 0.5 $m^2/s$, for example, $H_S$ was 0.63 for 1 m DEM, reducing to 0.15 with the 10 m DEM.

As described in the results, some simulations didn't converge to the stopping criteria. Non convergence was more common for D8 algorithm, due to the distribution of the volumes to fewer flow paths. The lower divergence of flow in D8 might result in pixels with unrealistic high flow depths, promoting flow even in gentle slopes. If the slope is too gentle and the flow height is too high, the volume exchange between cells might be just enough to be higher than the stopping criteria for thousands of iterations. Thus, a high count of false positives was observed for MFD and $D_\infty$ under lower values of kinematic viscosity.

### 5.2 Simulations with different rheological approaches

Simulations using the dilatant rheology approach, resulted in the most significant variation in performance for *v* values 0.05 and 0.1 $m^2/s$. Since these viscosities remain between the best and worst performances, the *n* coefficient becomes more important. At a viscosity of 0.1 $m^2/s$, for example, the lowest performance occurs within the lowest *n*, while the best result is achieved with the highest *n* value. For *n* of 2.0 and 1.2, the *TPR* ranged from 87 % to 88%, while the *FPR* ranged from 18% to 32.6%. In this case, the lowest speeds provided by the n of 2.0 controlled the number of false positives. For a viscosity of 0.5 $m^2/s$, however, the succession of performances was almost reversed, indicating that increased values of *n* greatly delayed the flow, reducing travel distance and leading to a lower true positive rate.

Regarding Bingham plastic, the parameter *z'* had a small influence of the model performance in the simulated scenarios. The variations considered in this study did not result in a relevant change in behavior. When comparing the simulated debris flow path with higher *z'*, it is possible to notice a slight reduction in the width. As flow height at debris flow's borders tend to be lower, the condition that allows a cell to outflow exclusively if accumulated height exceeds *z'* forces a reduction in debris flow width. Higher plug heights would be expected to end the simulation faster for this type of fluid, as pixels with height values below this value would not flow. This logic, however, was not confirmed. When comparing simulations, the higher *z'* sometimes went through more iterations before the simulation ended. One of the possible explanations is the reactivation of cell movement. With larger *z'*, more volume is stored in the cell, and when receiving a contribution from another pixel, its speed when reactivating the movement is faster than lower *z'*. As a result, the plug may have contributed to the stopping criteria not being met as easily.

The simulations tended to result in better $H_S$ for higher values of *v*, especially between $1\times10^{-2}$ and $1\times10^{-1}$. This might indicate high concentration of solids in the debris flow mixture, high bed resistance to flow, or a

https://doi.org/10.5194/nhess-2023-119
Preprint. Discussion started: 8 August 2023




combination of both. Therefore, this could be an implicit account for the absence of normal stress effects into the velocity-dependent parameter *v* (Naef et al., 2006). A comparison of flow velocities for different rheological approaches highlighted a limitation of the fixed time step: in steeper sections, the flow velocities would be high enough to outflow more than the available volume in the 1 s interval. Therefore, mean velocities tended to be as high as 1 m/s at the start of the simulation (despite the calculated instantaneous velocity being higher), as cells had 1 $m^3$ of volume. Consequently, the effect on velocity by different rheology was partially hindered by the fixed time step.

Although the rheological characteristics of the fluid are of fundamental importance in understanding the transport processes (Iverson, 2003), regarding the affected area, the effect of different rheological approaches was less significant than using different flow direction algorithms. In this way, by changing the fluid's viscosity, all the rheologies were able to represent the simulated flows.

**5.3 Validation scenarios**

For F2 and F3, false positives had a significant impact on the *Hs*, as the simulated debris flows extrapolated the observed scar's limits. However, the following factors may have affected the simulation's performance: (i) the presence of dense vegetation in the imagery may conceal the debris flow - the flow assumed heights lower than 30 cm at the end of the patch, so it could have easily continued between vegetation without damaging it; (ii) the shape of the scar and the simulated debris flow are similar for the F2 flow, but they do not overlap when the direction changes abruptly (from northeast to northwest) - this fact can be attributed to errors in the visual delimitation of the scar or a misrepresentation of the topography in the DEM. Also, some of limitations inherent to the model assumptions, especially regarding the laminar flow solutions and the absence of an erosion module, may have contributed to reduce its performance.

The worst performance of simulated flows was obtained by the F4 scenario. The *TPR* of this simulation was 58.20 %, with an *FDR* of 70%, indicating that most of the simulation is composed of false positives, which is the main reason for the lowest *Hs*, at 0.22. F4 simulated runout is noticeably different from the observed (Figure 6). Whereas the observed F4 debris flow scar changes direction, creating a meander, the simulated debris flow course is rather rectilinear. Also, the simulated scenario passes through a topographic constriction that leads to a high accumulation of volume, leading deposits of nearly 3 m of height. This accumulation area is flatter and does not distribute enough volume to surpass the stopping criteria, creating an unrealistic deposit in the middle of the transport area. In field surveys, this constriction was not observed and is probably a DEM preprocessing artifact. The simulation ends after forming a fan-shaped spread near the channel.

When calibrating their model, using an MDT of 10 m, Chiang et al. (2012) achieved *TPR* values of 92 % for the transport area and 88 % for the deposition area using the Newtonian approach coupled with $D_\infty$. The authors later applied the model to a 116 km² basin and obtained a *TPR* of 80%, accounting for the initiation, transport, and deposition areas all together. Gregoretti et al. (2016), achieved 83% *TPR* in their simulations for a debris flow occurring in the Lazin River basin, in the province of Trento, Italy, using a DEM with a resolution of 1 m. Regarding more robust models, Yamanoi et al. (2020) developed a model based on dilatant solutions of Takahashi (2014) and reached *TPR* from 0.570 to 0.741 for debris flow flooded areas in Northern Kyushu, Japan. Lee et al.

https://doi.org/10.5194/nhess-2023-119
Preprint. Discussion started: 8 August 2023




(2022), when comparing the effects of erosion models, for Bingham rheology, reached a *TPR* of 81.3% and 92.9% for two debris flow that occurred in Umyeon Mountain, Seoul, South Korea. Abraham et al. (2021) applied RAMMS to debris flows of Wayanad district of Kerala State, India and the *TPR* ranged from 0.286 to 0.416. Bout et al. (2018) reached a Cohen's kappa (equivalent to $H_S$) of 0.638 for a catchment scale simulation with LISEM, which considers both erosion and deposition during debris flow runout. Thus, the model was able to achieve *TPR* values comparable to more complex models in terms of affected area.

## 6 Conclusions

Debris flow modeling stands as a challenge due to the complexity of concerning processes and difficulty to observe and record them. In countries that lack extensive study of debris flow and field monitoring, such as Brazil, this challenge is especially difficult to overcome. This context reinforces the need to develop means to assess debris flow hazard with reliability. This study evaluated effects of different rheological approaches and flow direction algorithms on a model that requires few parameters to be utilized.

In terms of flow direction algorithms, D8 proved to be unsuitable for debris flow routing, whereas MFD performed better for high resolution DEM (1 m pixel size) and $D_\infty$ for coarser resolutions (2.5, 5 and 10 m). MFD presented better performance for debris flow F1 for the original DEM resolution of 1 m. The MFD can spread the flow to any surrounding pixel, therefore, reproducing more realistically the behavior of debris flow on flatter slopes. However, in lower resolutions the flow spreading of MFD becomes a limitation. Furthermore, on steeper slopes, especially near the initiation zone, there is an overestimation of the affected area due to excessive flow spreading. The DEM resolution has a strong effect over the simulations and affects how accurately the FD algorithm represents the debris flow path. MFD has lower performance as pixel size increases, conversely D8 has an increase in performance. $D_\infty$ performance change is mixed: there is a window where it rises, being 2.5 m the best performance, but as the pixel size increases the performance decreases.

The best results were obtained by dilatant rheology with *n* of 1.2 and Herschel-Bulkley with *m* of 0.6 and plug of 10 cm, both considering a kinematic viscosity of 0.5 $m^2/s$. These two rheological approaches have significant different behaviors, but rocky debris evidence obtained during field surveys suggests that the flows in the region may behave as dilatant. Thus, this set of parameters was applied to three other flows, achieving 84 % *TPR* and *Hs* of 0.52 for F2 and F3, which were simulated together, and % *TPR* for F4. The *TPR* for flows F1, F2, and F3 are equivalent to models with similar and more robust frameworks. The lack of data about debris flow velocities and height of depositions limited the comparison between the different rheological approaches. Therefore, further tests to verify the reliability of velocity and depth estimates are necessary.

The presented model is simple to calibrate since it requires few parameter inputs. It stands in the threshold between a physically based model and a topographic descriptor, allowing for quick assessment of debris flow in areas with limited data and information. The model results can be used to verify areas prone to debris flow by providing information on volume distribution and flow velocities. However, deposition heights and flow velocities are calculated using simplified mathematical approaches and should be interpreted accordingly. For further studies towards models with similar frameworks, a better solution for the stopping criteria is required. This can be accomplished by incorporating modules that simulate erosion and deposition while still allowing for the assessment

https://doi.org/10.5194/nhess-2023-119
Preprint. Discussion started: 8 August 2023




of debris flows from the initiation zone to deposition even in the absence of information such as debris flow hydrographs. Also, this model uses initiation areas as inputs and can be easily coupled with methodologies that map areas prone to landslide triggering.

**Code availability**

The code developed and utilized in this study can be accessed, edited, and downloaded at DOI: 10.5281/zenodo.8136370. To request additional information, please contact the corresponding authors.

**Data availability**

The data can be provided by the corresponding authors upon request.

**Author contribution**

LRP: conceptualization, investigation, methodology, software development, visualization, and writing – original draft, review and editing. GPM: conceptualization, data curation, and writing – review and editing. HS: visualization, writing – original draft, review and editing. BHA: writing – original draft, review and editing. CGS: writing – original draft, review and editing, visualization.

**Competing interests**

The authors declare they have no conflict of interests.

**Acknowledgments**

This research received financial support of CNPq - *Conselho Nacional de Desenvolvimento Científico e Tecnológico*. This research was undertaken by members of the GPDEN/IPH (*Grupo de Pesquisa em Desastres Naturais – Instituto de Pesquisas Hidráulicas*).

**References**

Abraham, M.T., Satyam, N., Reddy, S.K.P, Pradhan, B.: Runout modeling and calibration of friction parameters of Kurichermala debris flow, India, Landslides, 18(2), 737–754, https://doi.org/10.1007/s10346-020-01540-1, 2021.

Abraham, M.T., Satyam, N., Pradhan, B., Tian, H.: Debris flow simulation 2D (DFS 2D): Numerical modelling of debris flows and calibration of friction parameters, Journal of Rock Mechanics and Geotechnical Engineering, 14(6), 1747-1760. https://doi.org/10.1016/j.jrmge.2022.01.004, 2022.

Berti, M., Simoni, A.: DFLOWZ: A free program to evaluate the area potentially inundated by a debris flow. Computers and Geosciences, 67, 14–23. https://doi.org/10.1016/j.cageo.2014.02.002, 2014.

Bout, B., Lombardo, L., van Westen, C.J., Jetten, V.G.: Integration of two-phase solid fluid equations in a catchment model for flashfloods, debris flows and shallow slope failures, Environmental Modelling and Software, 105, 1–16, https://doi.org/10.1016/j.envsoft.2018.03.017, 2018.

https://doi.org/10.5194/nhess-2023-119
Preprint. Discussion started: 8 August 2023




Cabral, V., Reis, F.A., D'Affonseca, F.M., Lucía, A., Corrêa, C.V.S., Veloso, V., Gramani, M.F., Ogura, A.T., Lazaretti, A.F., Vemado, F., Filho, A.J.P.: Characterization of a landslide-triggered debris flow at a rainforest-covered mountain region in Brazil, Nat Hazards, 108, 3021–3043, https://doi.org/10.1007/s11069-021-04811-9, 2021.

Cabral, V., Reis, F., Veloso, V., Correa, C., Kuhn, C., Zarfl, C.: The consequences of debris flows in Brazil: a historical analysis based on recorded events in the last 100 years, Landslides, 20, 511-529, https://doi.org/10.1007/s10346-022-01984-7, 2023.

Cardozo, G.L., Zanandrea, F., Michel, G.P., Kobiyama, M.: Inventário de movimentos de massa na bacia hidrográfica do rio Mascarada/RS, Ci. e Nat., 43(31), https://doi.org/10.5902/2179460X43594, 2021.

Cavalli, M., Trevisani, S., Comiti, F., Marchi, L.: Geomorphometric assessment of spatial sediment connectivity in small Alpine catchments, Geomorphology, 188, 31–41, https://doi.org/10.1016/j.geomorph.2012.05.007, 2013.

Chen, L.C.: Generalized viscoplastic modeling of debris flow, J. Hydraulic Eng., 144, 237–258, 1988.

Chen, H., Lee, C.F.: Runout Analysis of Slurry Flows with Bingham Model, Journal of Geotechnical and Environmental Engineering, 128 (12), 1032-1042, https://doi.org/10.1061/ASCE1090-02412002128:121032, 2002.

Chiang, S.H., Chang, K., Mondini, A.C., Tsai, B., Chen, C.: Simulation of event-based landslides and debris flows at watershed level, Geomorphology, 138, 306–318, http://dx.doi.org/10.1016/j.geomorph.2011.09.016, 2012.

Fratini, P., Crosta, G., Carrara, A.: Techniques for evaluating the performance of landslide susceptibility models, Engineering Geology 111, 62-72, https://doi.org/10.1016/j.enggeo.2009.12.004, 2010.

Freeman, T.G.: Calculating catchment area with divergent flow based on a regular grid, Computers and Geosciences, 17, 413–422, https://doi.org/10.1016/0098-3004(91)90048-I , 1991.

Frey, H., Huggel, C., Bühler, Y., Buis, D., Burga, M.D., Choquevilca, W., Fernandez, F., García Hernández, J., Giráldez, C., Loarte, E., Masias, P., Portocarrero, C., Vicuña, L., Walser, M: A robust debris-flow and GLOF risk management strategy for a data-scarce catchment in Santa Teresa, Peru, Landslides, 13(6), 1493–1507, https://doi.org/10.1007/s10346-015-0669-z, 2016.

Gorr, A.N., McGuire, L.A., Youberg, A.M., Rengers, F.K.: A progressive flow-routing model for rapid assessment of debris-flow inundation, Landslides, 19(9), 2055–2073, https://doi.org/10.1007/s10346-022-01890-y, 2022.

Gregoretti, C., Degetto, M., Boreggio, M.: GIS-based cell model for simulating debris flow runout on a fan, Journal of Hydrology, 534, 326–340, http://dx.doi.org/10.1016/j.jhydrol.2015.12.054, 2016.

Han, Z., Su, B., Li, Y., Wang, W., Wang, W., Huang, J., Chen, G.: Numerical simulation of debris-flow behavior based on the SPH method incorporating the Herschel-Bulkley-Papanastasiou rheology model, Engineering Geology, 255, 26–36, https://doi.org/10.1016/j.enggeo.2019.04.013, 2019.

Heidke, P.: Berechnung des Erfolges und der Güte der Windstärkevorhersagen im Sturmwarnungdiens, Geografika Annaler, 8, 301–349, https://doi.org/10.1080/20014422.1926.11881138, 1926.

Horton, P., Jaboyedoff, M., Rudaz, B., Zimmermann, M.: Flow-R, a model for susceptibility mapping of debris flows and other gravitational hazards at a regional scale, Natural Hazards and Earth System Sciences, 13(4), 869–885, https://doi.org/10.5194/nhess-13-869-2013, 2013.

https://doi.org/10.5194/nhess-2023-119
Preprint. Discussion started: 8 August 2023




Huang, X., García, M.H.: A Herschel-Bulkley model for mud flow down a slope, Journal of Fluid Mechanics, 374, 305–333, https://doi.org/10.1017/S0022112098002845, 1998.

Hunt, B.: Newtonian fluid mechanics treatment of debris flow and avalanches, Journal of Hydraulic Engineering, 120, 1350–1363, https://doi.org/10.1061/(ASCE)0733-9429(1994)120:12(1350), 1994.

Hürlimann, M., Rickenmann, D., Medina, V., Bateman, A.: Evaluation of approaches to calculate debris-flow parameters for hazard assessment, Engineering Geology, 102(3–4), 152–163, https://doi.org/10.1016/J.ENGGEO.2008.03.012, 2008.

Iverson, R.M.: The debris-flow rheology myth, in: Debris flow hazards mitigation: mechanics, prediction, and assessment, 3rd International Debris-Flow Hazards Mitigation Conference, Davos, Switzerland 10-12 September 2003, 303-314, , ISBN 90 77017 78 X, 2003.

Jan, C.D., Shen, H.W.: Review dynamic modeling of debris flows In: Recent Developments on Debris Flows, edited by: Armanini, A., and Michiue, M., Springer Berlin, Heidelberg, Germany, 93–116, https://doi.org/10.1007/BFb0117757, 1997.

Kaitna, R., Rickenmann, D., Schatzmann, M.: Experimental study on rheologic behaviour of debris flow material, Acta Geotechnica, 2(2), 71–85, https://doi.org/10.1007/s11440-007-0026-z, 2007.

Kobiyama, M., Michel, G.P., Goerl, R.F.: Proposal of Debris Flow Disasters Management in Brazil Based on Historical and Legal Aspects, International Journal of Erosion Control Engineering, 11(3), 85–93. https://doi.org/10.13101/ijece.11.85, 2019.

Lee, S., An, H., Kim, M., Lee, G., Shin, H.: Evaluation of different erosion–entrainment models in debris-flow simulation, Landslides, 19(9), 2075–2090, https://doi.org/10.1007/s10346-022-01901-y, 2022.

Liu, W., He, S.: Comprehensive modelling of runoff-generated debris flow from formation to propagation in a catchment, Landslides, 17(7), 1529–1544. https://doi.org/10.1007/s10346-020-01383-w, 2020.

Liu, K.F., Huang, M.C.: Numerical simulation of debris flow with application on hazard area mapping, Computational Geosciences, 10(2), 221–240, https://doi.org/10.1007/s10596-005-9020-4, 2006.

Melo, R., Zêzere, J.L.: Modeling debris flow initiation and run-out in recently burned areas using data-driven methods, Natural Hazards, 88(3), 1373–1407, https://doi.org/10.1007/s11069-017-2921-4, 2017.

Mergili M., Krenn J., Chu H.J.: R.randomwalk v1, a multi-functional conceptual tool for mass movement routing, Geoscientific Model Development, 8(12), 4027–4043, https://doi.org/10.5194/gmd-8-4027-2015, 2015.

Naef D., Rickenmann D., Rutschmann P., Mcardell B.W.: Comparison of flow resistance relations for debris flows using a one-dimensional finite element simulation model, Nat. Hazards Earth Syst. Sci., 6, 155-165, https://doi.org/10.5194/nhess-6-155-2006, 2006.

Nakatani, K., Wada T., Satofuka Y., Mizuyama T.: Development of Kanako 2D (Ver. 2.00) a user-friendly one- and two-dimensional debris flow simulator equipped with a graphical user interface, International Journal of Erosion Control Engineering, 1(2), 62–72, http://dx.doi.org/10.13101/ijece.1.62, 2008.

O'Callaghan J.F., Mark, D.M.: The extraction of drainage networks from digital elevation data, Computer Vision, Graphics and Image Processing, 28, 323–344, http://dx.doi.org/10.1016/S0734-189X(84)80011-0, 1984.

Pellegrino A.M., Schippa L.: A laboratory experience on the effect of grains concentration and coarse sediment on the rheology of natural debris-flows, Environmental Earth Sciences, 77, 749, https://doi.org/10.1007/s12665-018-7934-0, 2018.

https://doi.org/10.5194/nhess-2023-119
Preprint. Discussion started: 8 August 2023




Phillips C.J., Davies T.R.H.: Determining rheological parameters of debris flow material. Geomorphology 4:101-110, 1991.

Pirulli M., Sorbino G.: Assessing potential debris flow runout: A comparison of two simulation models. Natural Hazards and Earth System Science, 8(4), 961–971. https://doi.org/10.5194/nhess-8-961-2008, 2008.

Pitman E.B., Nichita C.C., Patra A., Bauer A., Sheridan M., Bursik M.: Computing granular avalanches and landslides. Physics of Fluids, v. 15, n. 12, p. 3638–3646, 2003.

Rickenmann D., Laigle D., McArdell B.W., Hübl J.: Comparison of 2D debris-flow simulation models with field events. Computational Geosciences, 10(2), 241–264. https://doi.org/10.1007/s10596-005-9021-3, 2006.

Schippa L.: Modeling the effect of sediment concentration on the flow-like behavior of natural debris flow. International Journal of Sediment Research, 35(4), 315–327. https://doi.org/10.1016/j.ijsrc.2020.03.001, 2020.

Schwarz H., Michel G.P., Zanandrea F., Paul L.R., Salvador C.G.: Uso de caracterização morfométrica e geomorfológica na análise de mapeamentos de cicatrizes de escorregamentos. Revista Brasileira De Geomorfologia, 24(1). https://doi.org/10.20502/rbg.v24i1.2185, 2023.

~~Kobiyama M., Fan F.M., Michel, G.P., Tschiedel A., Zanandrea F., Paixão M.A., Godoy, J.V.Z.: Diagnóstico Preliminar: Descritivo dos eventos ocorridos no dia 5 de janeiro de 2017 entre as regiões dos municípios de São Francisco de Paula e Rolante/RS. Technical Report, Governo do Estado do Rio Grande do Sul, Brasil, 2017.~~

Steger, S., Scorpio, V., Comiti, F., Cavalli, M.: Data-driven modelling of joint debris flow release susceptibility and connectivity, Earth Surface Processes and Landforms, , 47(11), 2740-2764, https://doi.org/10.1002/esp.5421, 2022.

Takahashi T.: Debris Flow: Mechanics, Prediction and Countermeasures, 2nd ed, Taylor & Francis Group, London, England, https://doi.org/10.1007/s00024-008-0342-8, 2014.

Tang C., Zhu J., Chang M., Ding J., Qi X.: An empirical-statistical model for predicting debris-flow runout zones in the Wenchuan earthquake area, Quaternary International, 250, 63–73. https://doi.org/10.1016/j.quaint.2010.11.020, 2012.

Tarboton D.G.: A new method for the determination of flow directions and upslope areas in grid digital elevation models. Water Resources Research 33:309–319, 1997.

Yamanoi K., Oishi S., Kawaike K., Nakagawa H.: Predictive simulation of concurrent debris flows: How slope failure locations affect predicted damage, Journal of Flood Risk Management, 15(2), https://doi.org/10.1111/jfr3.12776, 2022.

Zhang Y, G. T, Tian W, L. YA.: Debris flow susceptibility mapping using machine-learning techniques in Shigatse area, China, Remote Sensing, 11(23), 2801, https://doi.org/10.3390/rs11232801, 2019.

https://doi.org/10.5194/nhess-2023-119
Preprint. Discussion started: 8 August 2023


Natural Hazards and Earth System Sciences
Discussions

555 **APPENDIX A**

**1. Mathematical model of dilatant fluid rheology**

The mathematical model for velocities of dilatant fluid rheology in a linear and steady state single-phase continuum debris flow is based on the following constitutive equation:

$$\tau = K_D \left(\frac{\partial u}{\partial z}\right)^n, n > 1 \quad (21)$$

$\tau$ is the shear stress [N/m²]; $K_D$ is dilatant consistency factor; $u$ is the is the velocity parallel to the surface [m/s] in
560 the $y$ position of the vertical component; $n$ is the flow index – higher values lead to a higher resistance to deformation according to the applied shear stress. A generalized velocity distribution from Chen (1988) model can be utilized to develop a solution for dilatant fluid. Chen (1988) model can be expressed by:

$$u = \left(\frac{n}{n+1}\right)\left(\frac{g.(h-z')^{n+1}.\sin\theta}{\nu_D}\right)^{\frac{1}{n}}\left[1-\left(1-\frac{y}{h-z'}\right)^{\frac{n+1}{n}}\right] \quad (22)$$

$z'$ adapts fluid's yield stress in function of a plug height [m] $\nu_D = K_D/\rho$, in which $\rho$ is the fluid density [kg/m³]; $g$ is the gravity acceleration [m/s²]; $h$ is the flow height [m]; $\theta$ is the slope angle [°]. For dilatant rheology, the yield
565 stress is negligible. Therefore, there is no plug in the surface of the flow and $z'$ can be neglected:

$$u = \left(\frac{n}{n+1}\right)\left(\frac{g.h^{n+1}.\sin\theta}{\nu_D}\right)^{\frac{1}{n}}\left[1-\left(1-\frac{y}{h}\right)^{\frac{n+1}{n}}\right] \quad (23)$$

Integrating Eq. (23) from 0 to $h$ and depth averaging we have a formulation for depth averaged velocity:

$$\frac{1}{h}\int_0^h u\,\partial y = U = \left(\frac{n}{n+1}\right)\left(\frac{g.h^{n+1}.\sin\theta}{\nu_D}\right)^{\frac{1}{n}}\left(1-\frac{n}{2n+1}\frac{h}{h}\right) \quad (24)$$

$$U = \left(\frac{n}{n+1}\right)\left(\frac{g.h^{n+1}.\sin\theta}{\nu_D}\right)^{\frac{1}{n}}\left(1-\frac{n}{2n+1}\right) \quad (25)$$